Polarization-insensitive and wide-angle broadband nearly perfect absorber by tunable planar metamaterials in the visible regime

2014 J. Opt. 16 125107

(http://iopscience.iop.org/2040-8986/16/12/125107)

IOP Publishing Journal of Optics
J. Opt. **16** (2014) 125107 (7pp) doi:10.1088/2040-8978/16/12/125107

Polarization-insensitive and wide-angle broadband nearly perfect absorber by tunable planar metamaterials in the visible regime

Xiaoyang Duan, Shuqi Chen, Wenwei Liu, Hua Cheng, Zhancheng Li and Jianguo Tian

The Key Laboratory of Weak Light Nonlinear Photonics, Ministry of Education, School of Physics and Teda Applied Physics Institute, Nankai University, Tianjin 300071, People's Republic of China

E-mail: schen@nankai.edu.cn and jjtian@nankai.edu.cn

Received 4 July 2014, revised 17 September 2014
Accepted for publication 22 October 2014
Published 27 November 2014

Abstract

We present the design and analysis of a polarization-insensitive and wide-angle broadband nearly perfect absorber by planar metamaterial in the visible regime. The bandwidth of absorption spectrum can be effectively expanded by combining multiple resonant elements. The forming mechanisms of the broadband metamaterial perfect absorber (MPA) are also demonstrated by the hybridization of the plasmonic system. The resonance of the broadband MPA can be dynamically tuned by varying the intensity of the incident beam. This kind of all-optically tunable perfect absorber will help to overcome some of the limitations of customary designs developed so far.

Keywords: perfect absorber, broadband, Kerr nonlinearity

(Some figures may appear in colour only in the online journal)

1. Introduction

Metamaterial perfect absorber (MPA), as one of the most fascinating anomalous high-efficiency light absorption based on plasmonic nanostructures, has aroused significant interest and attracted tremendous theoretical and experimental studies over the past few years [1–7]. They are typically composed of two structured metallic layers separated with a dielectric spacer, in which the electric and magnetic responses can be properly tuned by tailoring the structure. With the simultaneous realization of the impedance matching condition and the suppression of transmission, no energy is reflected and transmitted. Many efforts have been made to achieve MPA with polarization-insensitive, wide-angle, multi-band or broadband performance from gigahertz through terahertz to optical ranges, which underlay lots of different potential applications, such as photodetectors [8], microbolometers [9], imagers [10], sensing [11], photovoltaic solar cells [12], and thermal emitter [13].

Since the first microwave MPA was demonstrated by Landy *et al* [1], many efforts have focused on the broadband performance of MPA. Based on strong electromagnetic resonances, most of the designs have highly absorption in specific resonant frequencies, so the bandwidth of these MPAs is often narrow. Recently, Wakatsuchi *et al* [14] demonstrated a customizable broadband MPA by use of conductively lossy cut-wires in gigahertz regime. Ye *et al* [15] and Grant *et al* [16] also proposed a design by stacking multilayer composite structures with different geometrical dimensions, which can realize a polarization insensitive MPA in the terahertz range. Cui *et al* [17] presented a broadband absorber made of sawtoothed anisotropic metamaterial in infrared regime. By varying the geometric parameters of different components and packing them closely in the unit cell, all distinct narrow band resonant frequencies can be combined together obtaining a broadband MPA. However, these designs need to precisely align between the layers or stack multilayer composite structures, which complicate the

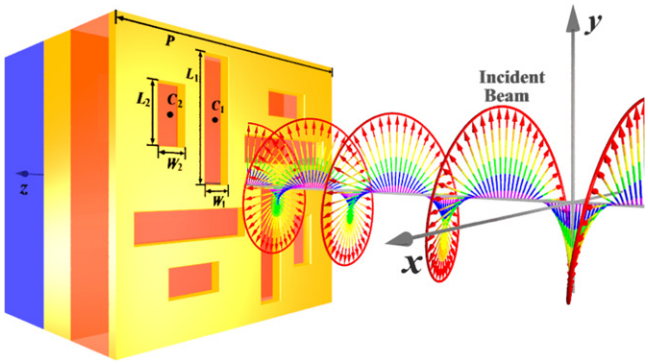

Figure 1. Unit cell of the designed MPA showing the geometry parameters: $P = 500$ nm, $L_1 = 220$ nm, $L_2 = 100$ nm, $W_1 = 50$ nm, and $W_2 = 50$ nm. The coordinate of the two cut-out slots are $C_1(65, 110)$ nm and $C_2(155, 110)$ nm.

fabrication process. Chen *et al* [18] and Hendrickson *et al* [19] also theoretically and experimentally demonstrated a kind of broadband planar MPA with multiplexed plasmonic nanostructures, which does not need to stack multilayer composite structures. However, they may only be tuned to different wavebands by carefully reoptimizing the geometry parameters owing to the reliance on resonances, which limits the potential applications of MPAs.

Recently, dynamically tunable and nonlinear properties are one of the most exciting areas in metamaterials research, which can overcome some limitations of custom designs and add a large degree of flexibility to the exotic properties [20–25]. By incorporating tunable-materials such as semiconductors [20], superconductors [21], transition oxide films [22], graphene [23] and nonlinear materials [24, 25], the plasmonics resonance of this hybrid metamaterials can be tuned by external stimuli such as thermal, optical excitation, electric and magnetic fields. Here, we introduce the Kerr nonlinear material into the MPA due to the following facts: (i) the electromagnetic energy is highly localized in the dielectric layer, (ii) the resonant absorption peak is sensitive to refractive index of the dielectric layer, which will realize an all-optically tunable metamaterials by a low incident power.

In this paper, we propose the design and analysis of a broadband planar MPA in the visible regime, in which the Kerr dielectric material is incorporated as the spacer of the sandwich structure to tune the resonant wavelength of the MPA. The bandwidth of absorption spectrum can be effectively expanded by combining multiple resonant elements. The forming mechanisms of the broadband MPA are demonstrated by the hybridization of the plasmonic system. Varying the intensity of the incident beam, the resonance of the broadband MPA can be dynamically tuned without the need to re-optimize or re-fabricate the nanostructures while maintaining high and broadband perfect absorption. The proposed broadband MPA is also polarization-insensitive and the absorption remains high even at large incident angles.

2. Design of the broadband planar MPA

The proposed broadband planar MPA is designed on a quartz substrate with permittivity of 2.25, as shown in figure 1, which consists of two gold layers separated by a layer of 120 nm thick Kerr dielectric spacer. The optical constants of gold in the visible regime are described by the Drude model with the relative permittivity at infinite frequency $\varepsilon_\infty = 9.0$, the plasma frequency $\omega_p = 1.3166 \times 10^{16}\ s^{-1}$, and the damping constant $\gamma = 1.3464 \times 10^{14}\ s^{-1}$ [26]. Most studies indicate that main energy is restricted in dielectric region between two metallic layers, so we introduce Kerr nonlinearity into the interlayer of our structure to realize an all-optically tunable MPA. The Kerr dielectric is decided by $\varepsilon_{Kerr} = \varepsilon_l + \chi^{(3)} |\mathbf{E}|^2$ with the linear dielectric constant $\varepsilon_l = 2.25$ and third-order susceptibility $\chi^{(3)}$. The top layer consists of four rotationally mixed-slots in a 20 nm thick homogeneous gold film. The thickness of the bottom gold layer is 100 nm, which is much larger than the typical skin depth of light in optical frequency, so the incident light cannot pass through the bottom layer. Thus, we only need to calculate the reflection (R) to get the structure absorption (A) using $A = 1 - R$, due to the transmission (T) is almost zero at all frequencies. Therefore, the key to obtain high absorption is to maximize the transmission of the top layer, which will maximize the interactions between upper and lower metallic layers, leading to the impedance match, and thus the structure absorption phenomenon will be improved. The finite element method based software of COMSOL Multiphysics [27] and the finite-difference time-domain method based Meep [28] were used to design the tunable broadband MPA and double-check the results each other. In the simulation, a y-polarized TEM beam is used as the excitation source, and periodic boundary conditions in all x–z and y–z planes are considered.

The resonant transmission properties in metallic slot array have been experimentally and theoretically investigated in recently years [29, 30]. There are two different but concomitant mechanisms responsible for the resonant transmission. First is the excitation of surface plasmon polaritons (SPPs), which is the direct result of periodical arrangement of the sub-wavelength structure. The SPPs is based on the interference of multiple waves scattered by slot array, and can be obviously affected by the properties of arrangement and thickness of dielectric interlayer. Second is the localized surface plasmon resonances (LSPRs), as either localized modes or localized waveguide resonances, is mostly due to the shape and size of the geometry in one lattice. Furthermore, as the wavelength increases, the dominant resonant transmission mechanism will change from SPPs to LSPRs. The proposed broadband MPA is based on metal–dielectric–metal multilayers. The bottom metal layer acts as an optical mirror to eliminate the transmittance. The top metal layer scatters electromagnetic waves and excites SPPs and LSPRs. The coupling between two metallic layers results in magnetic resonance depending on the dielectric constants of the dielectric spacer. The antiparallel currents are excited in the top and bottom gold layer. The circulating currents result in a

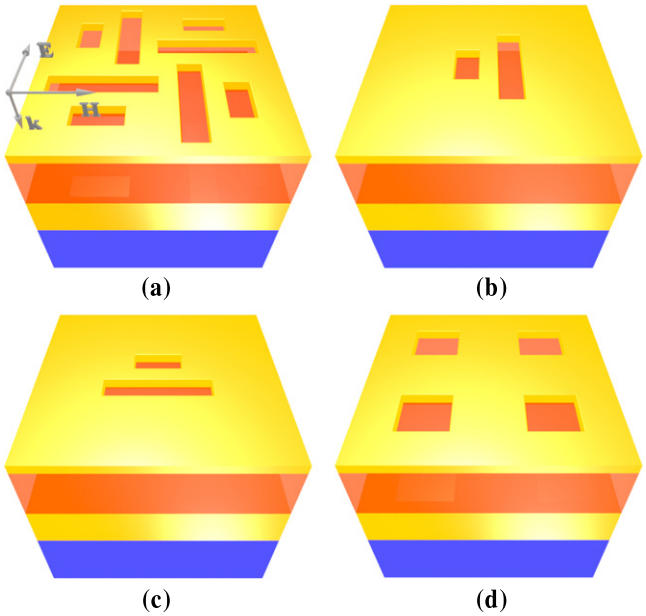

Figure 2. Unit cell of (a) the broadband MPA and its three decomposed nanostructures (b) mode 1, (c) mode 2, and (d) mode 3, respectively. The mixed-slots in (b) and (c) have same size with those in (a) and distribute in the center of the unit cell. The center of the square-slot is consistent with that of the mixed-slot in (a). The length of the square-slot is 100 nm.

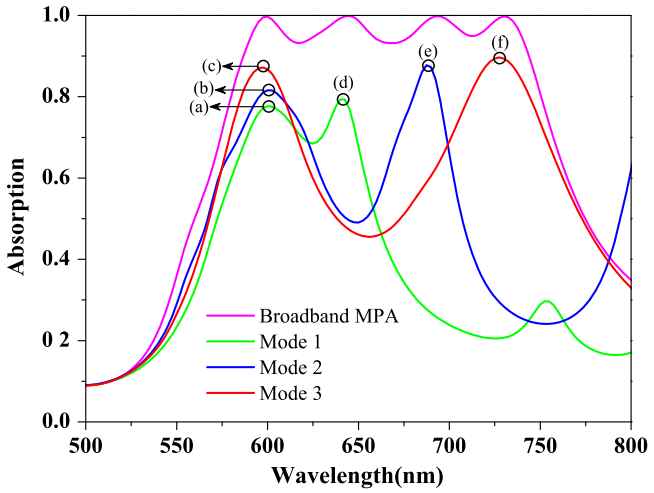

Figure 3. Simulated absorption spectra as a function of wavelength for the broadband planar MPA and three decomposed nanostructures.

magnetic moment which can strongly interact with the magnetic field of the incident light. To better analyze the forming mechanisms of the proposed broadband perfect absorber, we decomposed the broadband planar MPA into three nanostructures, which represent three kinds of mode, as shown in figure 2. Mode 1: the mixed-slot parallel to polarization; mode 2: the mixed-slot perpendicular to polarization; mode 3: the equivalent square-slot array. The coupling and interaction of hybrid plasmonic system provide feasible and efficient ways to manipulate the photons and tailor the optical response of system. So the mixed-slot array can be equivalent to a square-slot array to demonstrate the group effect in the composite structure. The rotational symmetry with polarization-independent response will significantly improve the surface plasmonic resonance and greatly extend their use in many fields.

3. Results and discussion

An incident beam with weak intensity was firstly used as the excitation source. Then, the nonlinearity of Kerr dielectric can be neglected, which is described as $\varepsilon_{\mathrm{Kerr}} = \varepsilon_1$. The simulated absorption spectra as a function of wavelength for the broadband planar MPA and three decomposed nanostructures are shown in figure 3. A nearly perfect absorption is observed for the proposed broadband planar MPA with four resonant peaks at $\lambda_1 = 599$ nm, $\lambda_2 = 645$ nm, $\lambda_3 = 693$ nm, and $\lambda_4 = 730$ nm, respectively. For each decomposed nanostructure, there are two main different absorption peaks, which correspond to SPPs and LSPRs, and the corresponding resonant wavelength is defined as λ_- and λ_+, respectively. The third resonance in the mode 1 corresponds to the high-order resonance of the SPPs. The intensity of the high-order resonance is very weak, which can not affect the whole absorption spectrum especially in the composite nanostructure. Therefore, we ignored the effect of the high-order resonance in the discussion. For the mode 1, the SPPs and LSPRs resonant wavelength are approximately at λ_1 and λ_2, namely $\lambda_- \approx \lambda_1$ and $\lambda_+ \approx \lambda_2$ (points (a) and (d) in figure 3); for the mode 2, there are $\lambda_- \approx \lambda_1$ and $\lambda_+ \approx \lambda_3$ (points (b) and (e) in figure 3); for the mode 3, there are $\lambda_- \approx \lambda_1$ and $\lambda_+ \approx \lambda_4$ (points (c) and (f) in figure 3). In case of the SPPs resonant wavelength (λ_-), the antiparallel currents are excited in the top and bottom gold layer. The circulating currents result in a magnetic moment which can strongly interact with the magnetic field of the incident light. A strong electromagnetic field is localized in the dielectric spacer, and the reflection is very weak. Consequently, electromagnetic energy can be efficiently confined in the nonlinear spacer. In the case of localized resonant wavelengths (λ_+), a strong electromagnetic field is established at the resonant wavelengths and localized in the dielectric spacer. The incident optical energy is neither transmitted nor reflected, thereby leads to nearly perfect absorbance of the proposed broadband MPA. In the proposed broadband MPA, if three elements of the structure (i.e. three modes showed in figure 2) are far enough from each other, the total absorption must be a single summation of the three effects. In this case, the broadband MPA cannot be formed. To get a nearly perfect broadband absorber, we optimize the structure carefully, and the three elements are close to each other. Then the coupling between three types of resonant elements will occur somehow. However, the basic resonances at each peak remain almost the same as the corresponding mode. The resonant peaks of the three modes finally merge into the broadband absorption spectrum of the planar MPA due to the coupling between each resonant element, which demonstrates the hybridization of the plasmonic system.

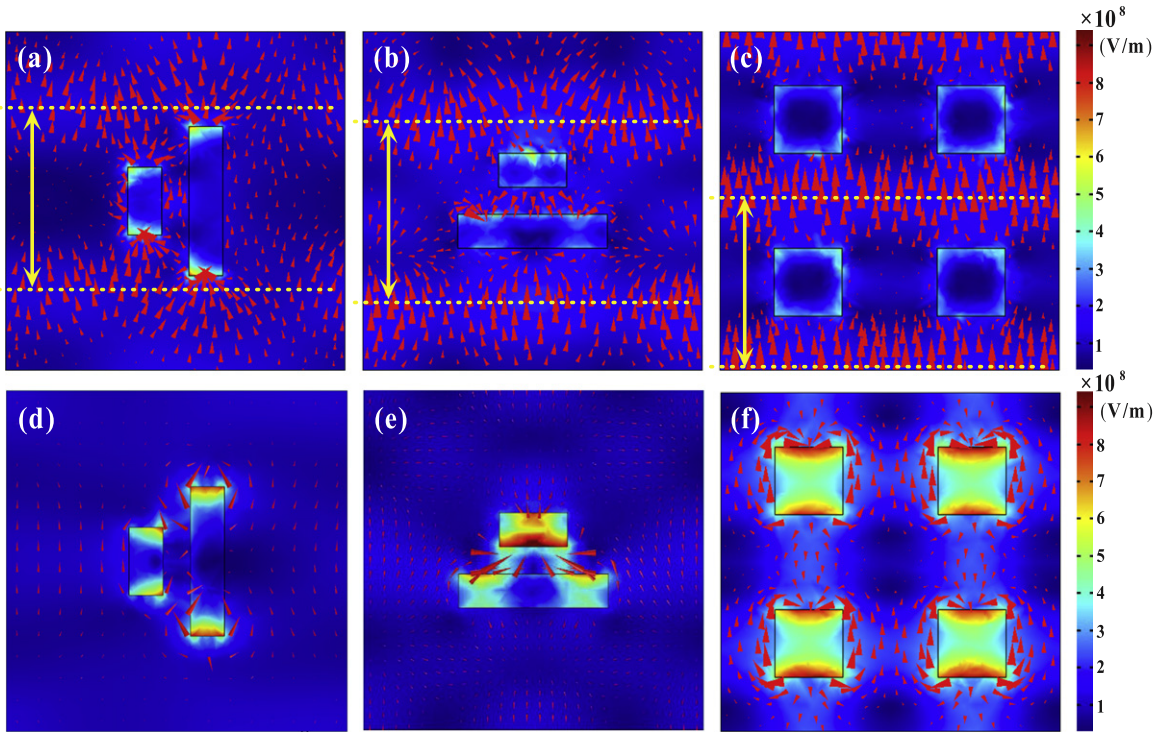

Figure 4. Calculated the electric field amplitude and surface current density distribution of the top gold layer at the resonant wavelengths of three modes, corresponding to the absorption peak (a)–(f) in figure 3, respectively. The yellow dot lines in (a)–(c) indicate the peaks of surface waves.

To get insight into the nature of three modes, we calculated the electric field amplitude and surface current density distribution of the top gold layer at the resonant wavelengths of three modes in figure 4, corresponding to the absorption peak (a)–(f) in figure 3. Each mode has two kinds of resonance. Left and right absorption peaks are formed by the SPPs resonance and the LSPRs, respectively. The SPPs resonant wavelengths of three modes are approximately at λ_1, which means the SPPs of three modes are the same as each other. The current density of three modes has also the same distribution, in which the peaks of surface waves are marked by yellow dot lines in figures 4(a)–(c). The LSPRs resonant wavelengths are determined by the shape of the mixed-slot. The incident beam can excite different resonant wavelengths at λ_2, λ_3, and λ_4 for different mixed-slots, respectively. A strong electric field and high surface current densities around the mixed-slots can be seen in figures 4(d)–(f), which means the energy can be constrained in specially localized areas at different wavelengths. The dominant resonant mechanisms can easily be distinguished by the surface current density distributions of three modes. As a result, four absorption peaks of more than 99% can be achieved by combining three different modes. The absorption bandwidth greater than 90% can reach 160 nm in visible regime.

To get a further analysis of the mechanisms of the proposed broadband nearly perfect absorption, we calculated the absorption spectra by varying the key geometry parameters of the broadband MPA in figure 5. As the increasing of the slot length L_1 from 180 nm to 240 nm, the absorption spectra can be further broadened and have a red shift, as shown in figure 5(a). The mixed-slot perpendicular to polarization for the mode 2 and the equivalent square-slot for the mode 3 can function as the magnetic dipole antenna at the localized resonant wavelength λ_+. Therefore, the absorption peaks at λ_3 and λ_4 have a red shift as the slot length L_1 increases. While, the absorption peak at λ_1 is not affected by varying the mixed-slot because of the SPPs. Then, the bandwidth of absorption spectra is finally broadened. As the decreasing of the thickness of the dielectric spacer from 120 nm to 90 nm, the absorption spectra can also be broadened and have a blue shift, as shown in figure 5(b). For three modes at the SPPs resonant wavelength λ_-, which is based on the coupling between the top gold film and the bottom gold plane, the resonant wavelength is dependent on the thickness of the dielectric spacer. Therefore, the absorption peaks at λ_1 have a blue shift as the decreasing of the thickness of dielectric spacer. These results show that the absorption spectra can be tuned by arranging the key geometry parameters of the broadband MPA, which confirms the validity of our design.

To analyze the influence of the dielectric spacer on the absorption band, we calculated the absorption spectra for the different linear dielectric constants ε_1 of the dielectric spacer in figure 6(a). In the linear case of the dielectric spacer, when the dielectric constant ε_1 is increasing from 2.25 to 2.75, the positions of absorption peaks almost linearly vary and have a red shift of about 40 nm, though the structure absorption is deteriorated a little due to the impedance mismatch. The simulation also shows that the electromagnetic field is highly enhanced and localized in the dielectric spacer at resonant frequencies. Therefore, if the Kerr dielectric material is

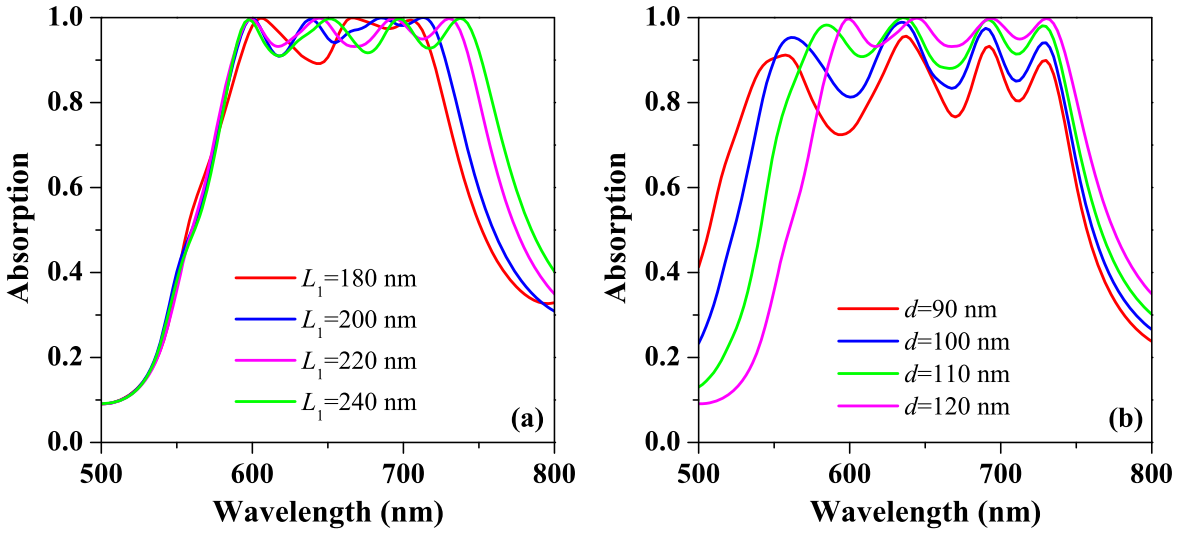

Figure 5. Simulated absorption spectra for the different (a) lengths L_1 and (b) thicknesses of the dielectric spacer d.

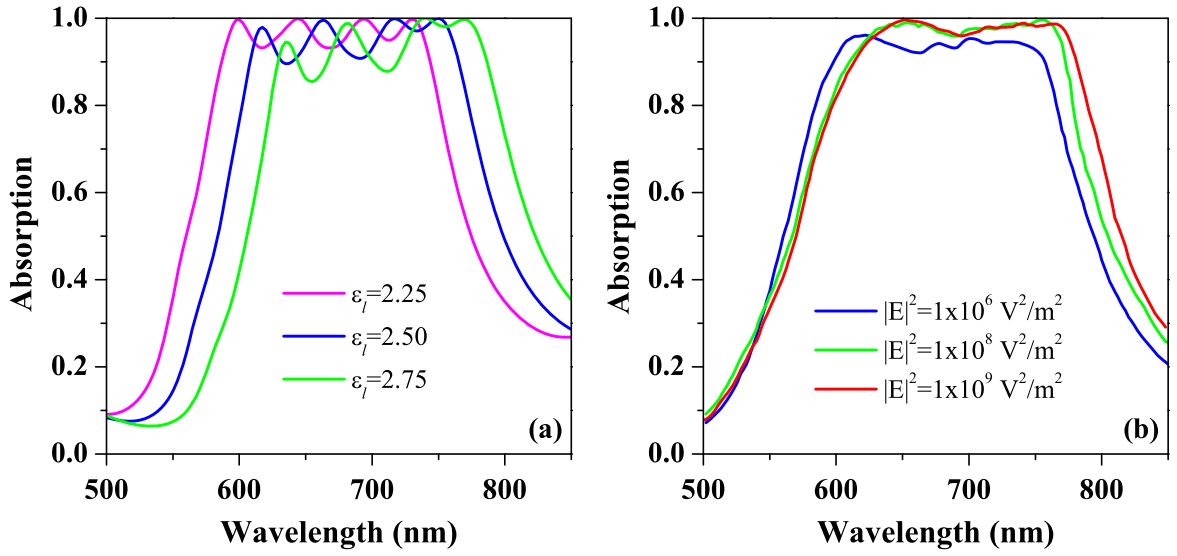

Figure 6. Simulated absorption spectra for the different (a) dielectric constants ε_l of the dielectric spacer and (b) incident intensities of a single continuous beam.

incorporated as the spacer of the broadband MPA, an all-optically tunable broadband MPA can be achieved in a lower incident power. In the nonlinear simulation, the Kerr dielectric is decided by $\varepsilon_{\text{Kerr}} = \varepsilon_l + \chi^{(3)} |\mathbf{E}|^2$ with the linear dielectric constant $\varepsilon_l = 2.25$ and third-order susceptibility $\chi^{(3)} = 9 \times 10^{-12}$ [25]. We simulated the absorption spectra excited by a single continuous beam with $|\mathbf{E}|^2$ of 1×10^6 V^2 m^{-2}, 1×10^8 V^2 m^{-2}, and 1×10^9 V^2 m^{-2}, in figure 6(b), respectively. With the increasing of optical intensity, the refractive index of the dielectric spacer is increasing obviously due to the Kerr nonlinear response, so the absorption spectra have an apparent red shift. As illustrated in figure 6(a), if the high enhancement of localized fields in structure is neglected, when $\varepsilon_{\text{Kerr}}$ increases from 2.25 to 2.75, the required intensity $|\mathbf{E}|^2$ should reach 5.56×10^{10} V^2 m^{-2} according to $\varepsilon_{\text{Kerr}} = \varepsilon_l + \chi^{(3)} |\mathbf{E}|^2$. The incident intensity is about one order of magnitude less than that of the absence of Kerr nonlinear material in the dielectric spacer as the drastic enhancement of the nonlinear optical response. In addition, the shape of the absorption spectra has a little difference with that of the absorption spectra in figure 6(a). It is because that the electric filed in the Kerr dielectric spacer is position dependent. Different positions own the different induced $\varepsilon_{\text{Kerr}}$, which will deteriorate the impedance match. Anyway, by varying the intensity of the incident beam, the resonance of the broadband MPA can be dynamically tuned without the need to re-optimize or re-fabricate the nanostructures while maintaining high and broadband perfect absorption.

Polarization-insensitive performance and wide-angle incident beams are important in practical applications. In some cases, the most possible light needs to be used, which may contain some arbitrarily polarized components. Moreover, the excited beam is not always normally incident to the sample in many cases. To show the polarization-insensitive

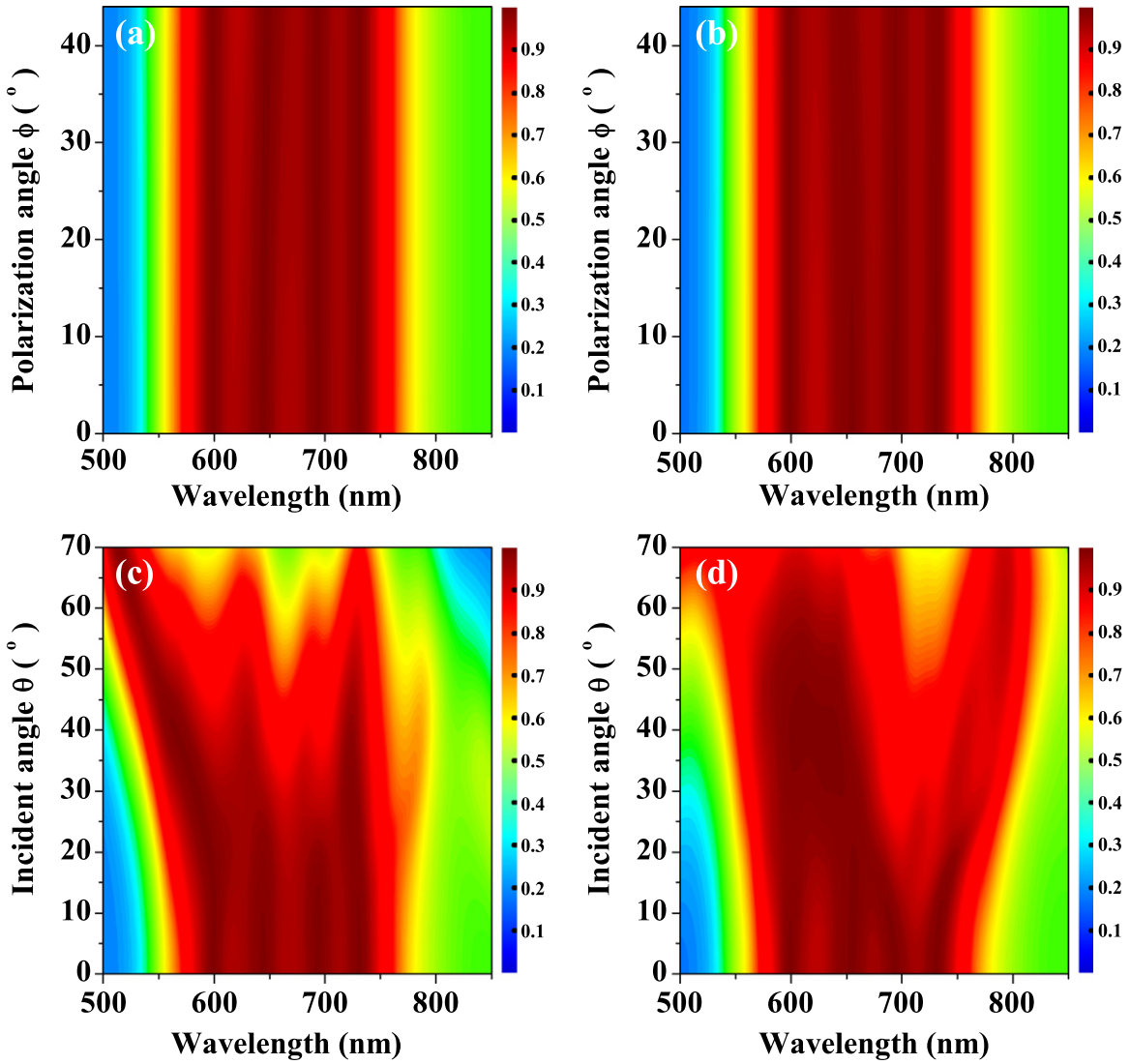

Figure 7. Simulated absorption spectra as a function of wavelength and the polarization angle for (a) TE and (b) TM polarization. Simulated angular dispersion of the absorption spectra for (c) TE and (d) TM polarization.

and wide-angle behaviors and wide-angle incident beam, we plotted the absorption spectra as a function of polarization angle ϕ for TE and TM polarization in figures 7(a) and (b), respectively. As the proposed broadband MPA has a fourfold rotational symmetry, we only need to take into account the polarizations from 0° to 45° in the simulation. Results show that the absorption spectra of the broadband MPA are polarization-insensitive. The angular dispersions of the absorption spectra are also simulated for TE and TM polarization in figures 7(c) and (d), respectively. The electric field plays more important role in driving the surface plasmonic resonance at optical frequency. The SPPs and LSPRs are still coexisting with increasing of the incident angle. However, they are differently affected as the incident angle increases. For the TE case, electric fields are still parallel to the metal surface, so the LSPRs (λ_2, λ_3, and λ_4) are hardly influenced within 40°. However, the delocalized resonance SPPs (λ_1) has a blue shift, because the effective thickness of the spacer is increasing as the incident angle increases. Therefore, the coupling between the top gold film and the bottom gold plane decreases, which will destroy the impedance match leading to the absorption significantly decrease. Meanwhile, the effective magnetic field becomes less and less, so the absorption gradually decreases when the incident angle beyond 40° due to the impedance mismatch. For the TM case, all resonances can still maintain well within 30°. But when the effective electric field becomes less and less with the increasing of incident angle, the electric resonance may not be efficiently driven any more. Therefore, the absorption gradually decreases when the incident angles vary from 30° to 70°. These results reveal that the proposed broadband MPA operates quite well for both TE and TM radiation over a wide range of incident angles.

As the proposed broadband MPA has good performance for practical applications, it would make sense to use experimental material parameters for simulations. To more clearly exhibit the difference of broadband MPA between using the experimental parameters [31] and Drude model, we

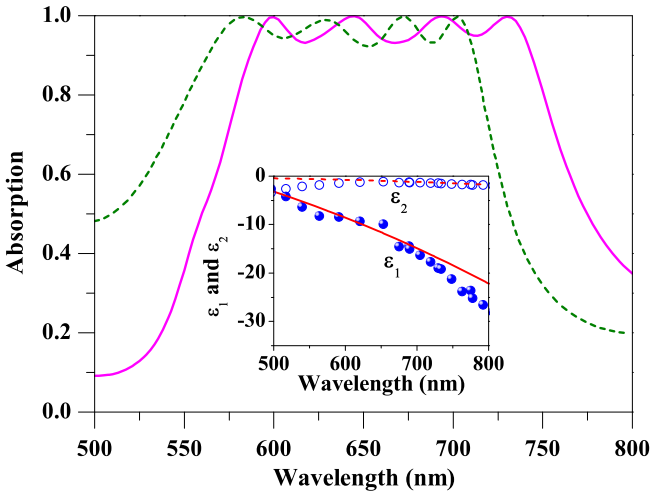

Figure 8. Simulated absorption spectra using the experimental parameters and Drude model. Inset: real (blue balls and red solid line) and imaginary parts (blue circles and red dashed line) of the dielectric function of gold for experimental parameters (blue balls and circles) and Drude model (red solid line and dashed line).

show the simulated absorption spectra for these two cases in figure 8. The imaginary part of the glass dielectric spacer is also considered as 10^{-5} in the simulation for the experimental parameter [31]. We can see that the characteristics of the broadband MPA still can be well kept except for a blue shift of 25 nm. The inset of figure 8 also shows the real and the imaginary parts of the dielectric function of gold for experimental results and Drude model. Results show that the real and the imaginary parts have a slight deviation in the long and the short wavelength for experimental results and Drude model, respectively, which mainly results in a blue shift of the broadband MPA.

4. Conclusions

In conclusion, we have numerically demonstrated a polarization-insensitive and wide-angle broadband MPA in visible regime composed of gold mixed-slot arrays, a Kerr dielectric spacer and a gold plane layer. The bandwidth of absorption spectrum can be effectively expanded by coupling of three kinds of modes. The resonance of the broadband MPA can be dynamically tuned by varying the intensity of the incident beam. This kind of all-optically tunable absorber will help to overcome some of the limitations of customary designs developed so far. Our work offers a further step forward in many potential applications in all-optical integrated photonic circuits, such as thermal detector and imaging, solar cell, and coating material to mitigate spurious reflections.

Acknowledgments

This work was supported by the Chinese National Key Basic Research Special Fund (2011CB922003), the National Basic Research Program (973 Program) of China (2012CB921900), the Natural Science Foundation of China (11304163 and 61378006), the Program for New Century Excellent Talents in University (NCET-13-0294), the Natural Science Foundation of Tianjin (13JCQNJC01900), the Specialized Research Fund for the Doctoral Program of Higher Education (20120031120032), and the 111 project (B07013).

References

[1] Landy N I, Sajuyigbe S, Mock J J, Smith D R and Padilla W J 2008 *Phys. Rev. Lett.* **100** 207402
[2] Watts C M, Liu X and Padilla W J 2012 *Adv. Mater.* **24** OP98
[3] Chen K, Adato R and Altug H 2012 *ACS Nano* **6** 7998
[4] Shen X, Yang Y, Zang Y, Gu J, Han J, Zhang W and Cui T J 2012 *Appl. Phys. Lett.* **101** 154102
[5] Tuong P V, Park J W, Rhee J Y, Kim K W, Jang W H, Cheong H and Lee Y P 2013 *Appl. Phys. Lett.* **102** 081122
[6] Zhang B, Zhao Y, Hao Q, Kiraly B, Khoo I C, Chen S and Huang T J 2011 *Opt. Express* **19** 15221
[7] Park J W, Tuong P V, Rhee J Y, Kim K W, Jang W H, Choi E H, Chen L Y and Lee Y P 2013 *Opt. Express* **21** 9691
[8] Shrekenhamer D, Xu W, Venkatesh S, Schurig D, Sonkusale S and Padilla W J 2012 *Phys. Rev. Lett.* **109** 177401
[9] Maier T and Brückl H 2009 *Opt. Lett.* **34** 3012
[10] Liu X, Starr T, Starr A F and Padilla W J 2010 *Phys. Rev. Lett.* **104** 207403
[11] Liu N, Mesch M, Weiss T, Hentschel M and Giessen H 2010 *Nano Lett.* **10** 2342
[12] Wang Y, Sun T, Paudel T, Zhang Y, Ren Z and Kempa K 2012 *Nano Lett.* **12** 440
[13] Liu X, Tyler T, Starr T, Starr A F, Jokerst N M and Padilla W J 2011 *Phys. Rev. Lett.* **107** 045901
[14] Wakatsuchi H, Greedy S, Christopoulos C and Paul J 2010 *Opt. Express* **18** 22187
[15] Ye Y Q, Jin Y and He S 2010 *J. Opt. Soc. Am.* B **27** 498
[16] Grant J, Ma Y, Saha S, Khalid A and Cumming D R S 2011 *Opt. Lett.* **36** 3476
[17] Cui Y, Fung K H, Xu J, Ma H, Jin Y, He S and Fang N X 2012 *Nano Lett.* **12** 1443
[18] Chen S, Cheng H, Yang H, Li J, Duan X, Gu C and Tian J 2011 *Appl. Phys. Lett.* **99** 253104
[19] Hendrickson J, Guo J, Zhang B, Buchwald W and Soref R 2012 *Opt. Lett.* **37** 371
[20] Chen H T, O'Hara J F, Azad A K, Taylor A J, Averitt R D, Shrekenhamer D B and Padilla W J 2008 *Nat. Photonics* **2** 295
[21] Lee H M and Wu J C 2012 *IEEE Trans. Magn.* **48** 4243
[22] Huang W, Yin X, Huang C, Wang Q, Miao T and Zhu Y 2010 *Appl. Phys. Lett.* **96** 261908
[23] Pu M, Chen P, Wang Y, Zhao Z, Wang C, Huang C, Hu C and Luo X 2013 *Opt. Express* **21** 11618
[24] Chen P Y, Farhat M and Alù A 2011 *Phys. Rev. Lett.* **106** 105503
[25] Gong Y, Li Z, Fu J, Chen Y, Wang G, Lu H, Wang L and Liu X 2011 *Opt. Express* **19** 10193
[26] Johnson P B and Christy R W 1972 *Phys. Rev.* B **6** 4370
[27] Comsol A B 2008 COMSOL Multiphysics User's Guide version 3.5 (Burlington, Mass)
[28] Meep 1.2 http://ab-initio.mit.edu/wiki/index.php/Meep
[29] Miyamaru F and Takeda M 2009 *Phys. Rev.* B **79** 153405
[30] Schwind M, Kasemo B and Zorić I 2013 *Nano Lett.* **13** 1743
[31] Palik E D 1998 *Handbook of Optical Constants of Solids* 3rd edn (Academic: New York)